Low-energy electron scattering by CH_3F, CH_2F_2, CHF_3, and CF_4

Márcio T. do N. Varella
Instituto de Física "Gleb Wataghin," Universidade Estadual de Campinas, UNICAMP, 13083-970 Campinas, São Paulo, Brazil

Carl Winstead and Vincent McKoy
A. A. Noyes Laboratory of Chemical Physics, California Institute of Technology, Pasadena, California 91125

Masashi Kitajima and Hiroshi Tanaka
Department of Physics, Sophia University, Tokyo 102-8554, Japan
(Received 22 January 2001; published 4 January 2002)

We present measured and calculated differential cross sections, as well as calculated integral cross sections, for elastic electron collisions with CH_3F, CH_2F_2, CHF_3, and CF_4. The calculated cross sections were obtained with the Schwinger multichannel method, and a Born-closure procedure was used to improve the differential cross sections for polar systems. Polarization effects were found to be relevant even for systems with moderately large permanent dipole moments, such as CH_3F and CHF_3. In general, there is good agreement between theory and experiment.

DOI: 10.1103/PhysRevA.65.022702 PACS number(s): 34.80.Bm

I. INTRODUCTION

In recent years, there has been increasing interest in the study of electron scattering by fluoromethanes, due to their importance to different fields such as plasma chemistry and astrophysics [1,2]. In particular, cross sections for electron scattering by fluoromethanes are crucial data in the modeling of low-temperature plasmas used in the semiconductor industry, and at least one of these molecules, CF_4, is of environmental concern [1].

In spite of their importance, electron-scattering data for fluoromethanes, especially theoretical data, are sparse. For CH_3F, measurements of the cross sections for ionization and fragmentation [3], dissociation [4], and total scattering [5,6] have been reported. For CH_2F_2, the total scattering cross section has recently been measured [7]; measured dissociation cross sections [4] and a calculated elastic-scattering cross section [8] are also available. Electron interactions with CHF_3 have been reviewed by Christophorou *et al.* [2]; in addition, measurements of the dissociation [4,9] and total scattering cross sections [10,11], as well an elastic-scattering calculation [12], have recently been reported. CF_4, on the other hand, is by far the most widely studied of the molecules considered here. Recently reported work includes measurements of the dissociation [4,13], ionization [13], and total collision [10] cross sections as well as elastic-scattering calculations [14–16]; earlier work has been reviewed by Christophorou *et al.* [1]. The so-called halogenation effect in the fluoromethane elastic differential cross sections—that is, the effect of successively replacing H atoms by F atoms in CH_xF_{4-x}—has been addressed recently both experimentally [17] and theoretically [18]. In view of these facts, a study on low-energy electron scattering by fluoromethanes is quite opportune.

Recalling that all fluoromethanes except CF_4 possess considerable permanent dipole moments, three main factors will determine the behavior of the low-energy electron-scattering cross sections: (i) fluorination effects, (ii) dipole moment magnitudes, and (iii) polarization effects. It is the purpose of the present paper to report measurements and calculations for elastic electron scattering by fluoromethanes, focusing on how elaborate calculations must be to reproduce experimental data. In other words, we aim to find out how important dipole-moment interactions and polarization effects are in the energy range considered here ($E<15$ eV). We believe such information to be valuable since description of polarization is far more computationally demanding than inclusion of longer-range ($\propto 1/r^2$) interactions.

Our calculated cross sections are obtained with the Schwinger multichannel (SMC) method [19,20] as implemented for parallel computers [21]. The use of large-scale parallel computers is of great help because the computational effort scales very rapidly as H atoms are replaced by F atoms and as configurations are added to account for polarization. Because the SMC method employs Cartesian Gaussian basis sets in the representation of not only the target but also the scattering wave function, one may study electron scattering by polyatomic targets of arbitrary geometry within a fully *ab initio* framework without relying on single-center expansions. However, because the trial wave function employed in the SMC method is square integrable, the long-range interaction of the projectile with a permanent dipole moment is not fully taken into account. An analogous problem arises in methods relying on single-center expansions: typically, only the contributions of the lowest several partial waves to the cross section are computed, but the dipole interaction remains significant at high partial waves. In order to overcome this difficulty, we adopt the well-known Born closure procedure [22,23], in which higher partial waves are described through the first Born approximation (FBA) applied to the point-dipole scattering potential. Although the Born closure approach improves differential cross sections (DCS) at small scattering angles ($\theta<30°$), it leads to an unphysical divergence in the forward-scattering direction ($\theta=0°$) if the point dipole is considered to be fixed in space, complicating the evaluation of integral cross sections (ICS). We avoid the di-

vergence at 0° by assuming a rotating dipole [24–27]; taking the rotational energy transfer into account removes the singularity in the DCS. Details of our approach will be given in Sec. II. With the dipolar interaction suitably described, we are able to compare static-exchange (SE) and static-exchange–plus–polarization (SEP) calculations to elucidate the role played by both longer-range and shorter-range interactions in the scattering process.

It should be observed that only some specific features of the above-mentioned fluorination effect have been previously considered [17]. The occurrence of prominent structures in the experimental elastic DCS was discussed only for collision energies of 1.5, 30, and 100 eV; many other intermediate impact energies are addressed in this report. Previously reported measurements for CF_4 [28] are included for comparison.

II. THEORY

A. Schwinger multichannel method

The SMC method has been described elsewhere [19,20] and here we only give the working expression for the scattering amplitude,

$$[f_{\vec{k}_f,\vec{k}_i}] = -\frac{1}{2\pi}\sum_{m,n}\langle S_{\vec{k}_f}|V|\chi_m\rangle (d^{-1})_{mn}\langle\chi_n|V|S_{\vec{k}_i}\rangle, \quad (1)$$

where

$$d_{mn} = \left\langle \chi_m \middle| \frac{\hat{H}}{N+1} - \frac{(\hat{H}P+P\hat{H})}{2} + \frac{(VP+PV)}{2} - VG_P^{(+)}V \middle| \chi_n \right\rangle. \quad (2)$$

In the above equations, $S_{\vec{k}_{i,f}}$ are solutions of the unperturbed Hamiltonian (molecular Hamiltonian plus the kinetic-energy operator for the incident electron); V is the interaction potential between the incident electron and the molecular target; $|\chi_n\rangle$ is an $(N+1)$-particle spin-adapted Slater determinant (a configuration state function); $\hat{H}$ is the total energy minus the full Hamiltonian of the problem; P is a projection operator onto the open-channel space defined by energetically accessible target states; and $G_P^{(+)}$ is the free particle Green's function projected onto this P space.

B. Born-closure procedure

Details of the Born-closure procedure have been discussed previously [29,30]. The basic idea is to employ a point-dipole potential to represent the electron-target interaction and then apply the first Born approximation (FBA) for a general rotational transition, $\Gamma \to \Gamma'$ (Γ denotes a complete set of rotational quantum numbers). In such cases, the scattering cross section is given by [25]:

$$f^{FBA}_{\Gamma\to\Gamma'}(\vec{k}_i,\vec{k}_f) = -\frac{1}{2\pi}\int d^3r \exp[i(\vec{k}'_{\Gamma'}-\vec{k}_\Gamma)\cdot\vec{r}] \times \int d\Omega \Psi^*_{\Gamma'}(\Omega)V(\vec{r},\Omega)\Psi_\Gamma(\Omega), \quad (3)$$

where $\Omega \equiv (\alpha,\beta,\gamma)$ are the Euler angles used to describe target orientation in the laboratory-fixed frame, and Ψ_Γ is a rotational eigenfunction of the target,

$$H_{rot}|\Psi_\Gamma\rangle = \epsilon_\Gamma|\Psi_\Gamma\rangle. \quad (4)$$

If V is simply the dipole moment interaction, integration over $\vec{r}$ is straightforward and leads to

$$f^{FBA}_{\Gamma\to\Gamma'}(\vec{k}_i,\vec{k}_f) = \int d\Omega \Psi^*_{\Gamma'}(\Omega) f^{FBA}(\vec{k}_i,\vec{k}_f)\Psi_\Gamma(\Omega), \quad (5)$$

with

$$f^{FBA}(\vec{k}_i,\vec{k}_f) = -\frac{i}{\pi}\frac{\vec{D}\cdot(\vec{k}_i-\vec{k}_f)}{|\vec{k}_i-\vec{k}_f|^2}. \quad (6)$$

In the above expressions, $\vec{D}$ is the molecular dipole moment, and $\vec{k}_i$ ($\vec{k}_f$) is the incoming (outgoing) wave-vector. It should be noted that the incident direction ($\hat{k}_i$) is a function of the target orientation in the molecule-fixed frame, $\vec{D}$ being assumed to coincide with the molecular symmetry axis. In the laboratory-fixed frame, on the other hand, $\hat{k}_i$ is defined by the incident beam, while $\hat{D}$ depends on the target orientation. The partial-wave expansion for f^{FBA} is also analytical and becomes increasingly accurate in the high partial-wave (i.e., large impact parameter) limit, $\ell \to \infty$. Accordingly, one is able to obtain an accurate partial-wave sum by replacing the lower partial-wave terms of Eq. (5) with those obtained through a more elaborate approximation. In the present paper, we use a combination of the SMC method with the adiabatic-nuclei approximation [31] as applied to rotation

$$f^{SMC}_{\Gamma\to\Gamma'}(\vec{k}_i,\vec{k}_f) = \int d\Omega\, \Psi^*_{\Gamma'}(\Omega) f^{SMC}(\vec{k}_i,\vec{k}_f)\Psi_\Gamma(\Omega), \quad (7)$$

where f^{SMC} is the SMC elastic-scattering amplitude, given by Eq. (1). From Eqs. (1), (5), (6), and (7) one obtains the Born-closure (BC) expression for the $\Gamma \to \Gamma'$ transition

$$f^{BC}_{\Gamma\to\Gamma'}(\vec{k}_i,\vec{k}_f) = \int d^3\Omega \Psi^*_{\Gamma'}(\Omega) f^{BC}(\vec{k}_i,\vec{k}_f)\Psi_\Gamma(\Omega), \quad (8)$$

where

$$f^{BC}(\vec{k}_i,\vec{k}_f) = f^{FBA}(\vec{k}_i,\vec{k}_f) + \sum_{\ell=0}^{\ell_{SMC}}\sum_{\mu=-\ell}^{\mu=\ell}[f^{SMC}_{\ell\mu}(\vec{k}_i,\vec{k}_f) - f^{FBA}_{\ell\mu}(\vec{k}_i,\vec{k}_f)]Y_{\ell\mu}(\hat{k}_f). \quad (9)$$

In the latter equation, $f^{SMC}_{\ell\mu}$ and $f^{FBA}_{\ell\mu}$ are, respectively, coefficients of expansion of Eqs. (1) and (6) in spherical harmonics $Y_{\ell\mu}$ in the laboratory-fixed frame, and ℓ_{SMC} is the high-

TABLE I. Number of configurations used in electron-fluoromethane scattering calculations in the static-exchange (SE) and static-exchange–plus–polarization (SEP) approximations.

C_S		A'	A''	C_{2v}		A_1	B_1	B_2	A_2
CH_3F	SE	56	27	CH_2F_2	SE	41	28	21	12
	SEP	2063	2065[a]		SEP	2071	2042	2007	12
CHF_3	SE	75	46	CF_4	SE	54	34	34	18
	SEP	2704	2710[b]		SEP	3223	2802	2802[c]	2459

[a] $A''=E_x$ (generated from A') $+A_2$ (2 SE configurations). See text.
[b] $A''=E_x$ (generated from A') $+A_2$ (6 SE configurations). See text.
[c] Generated from B_1. See text.

est partial wave described through the SMC method and is chosen to provide the smallest deviation from the pure SMC differential cross section for high scattering angles. The rotationally unresolved elastic-scattering cross section may now be calculated as the rotationally summed cross section [25] out of any initial rotational state [32,33], for example the ground state

$$\frac{d\sigma}{d\Omega}^{elas}(\theta_f)=\sum_{\Gamma}\frac{d\sigma}{d\Omega}^{0\to\Gamma}(\theta_f) \tag{10}$$

with

$$\frac{d\sigma}{d\Omega}^{0\to\Gamma}(\theta_f)=\frac{1}{2\pi}\frac{k}{k_\Gamma}\int_0^{2\pi}d\phi_f|\langle\Psi_\Gamma|f^{BC}|\Psi_0\rangle|^2. \tag{11}$$

Among the polar molecules addressed in this paper, CH_3F and CHF_3 are symmetric tops, whose rotational eigenfunctions are labeled by the quantum numbers J, K, and M, representing, respectively, the molecular angular momentum and its projections on the quantization axes of the molecule- and laboratory-fixed frames. It is well known [26,34] that the dipole-allowed rotational transitions for a symmetric top are governed by

$$J'=J\pm1;\quad K'=K=0, \tag{12}$$

and

$$J'=J;\quad K'=K\neq0. \tag{13}$$

Thus, the only dipole-allowed rotational excitation in the sum on the right-hand side of Eq. (10) is $(J=0K=0\to J'=1K'=0)$, with an associated energy transfer that prevents divergence of the dipole cross section. As a result, the elastic and momentum-transfer cross sections obtained as rotationally summed cross sections from the rotational ground state are also nondivergent.

At this point, however, a seeming contradiction arises, because elastic transitions $(\Delta J=0)$ would produce an infinite cross section if we were to choose any state other than $J=0,K=0$ as the initial state [26,35]. The resolution of the paradox lies in the observation that the divergence is due solely to elastic scattering at small angles. The divergent contribution to the small-angle scattering arises from distant collisions, or equivalently from high electron angular momenta; however, at any given collision energy, the adiabatic approximation must break down for a sufficiently large impact parameter, because the interaction time cannot remain small compared to the rotational period in such distant collisions. Consistent with this observation, the expressions developed by Crawford [26] for the Born cross sections of a dipole embedded in a symmetric top with a large moment of inertia show that, except at small scattering angles, the elastic and inelastic differential cross sections are essentially equal apart from a factor of $(2J'+1)/(2J+1)$. Consequently, the rotationally summed differential cross section is independent of the initial value of J—except, again, at small angles, where only the cross section for $J=0$ is nondivergent. Under these circumstances, it is reasonable to assume that the rotationally summed cross section out of the $(J=0,K=0)$ state is comparable to the experimental rotationally unresolved cross section.

III. COMPUTATIONAL PROCEDURES

All calculations were performed with the nuclei fixed at the experimental equilibrium geometry [36]. Both occupied and scattering orbitals were described with the $6-311++G(2d,2p)$ basis set internal to the electronic structure program GAMESS [37], augmented with diffuse s and p functions on the fluorine atoms, both with an exponent of 0.03587. It should be noted that all six Cartesian components of the d functions are included in the basis set.

In the static-exchange (SE) calculations, canonical Hartree-Fock (HF) virtual orbitals (VO's) were used as scattering orbitals. CH_2F_2 and CF_4 were considered in C_{2v} symmetry and CH_3F and CHF_3 in C_{3v} symmetry. The number of VO's belonging to each irreducible representation (IR) appears in Table I as the number of SE configurations. The procedure adopted for static-exchange–plus–polarization (SEP) calculations is as follows. The $(N+1)$-particle configuration spaces were built up considering only spin-preserving single excitations out of valence orbitals into compact sets of polarizing orbitals generated from the virtual orbitals and the canonical orbital energies [38] but using the entire set of VO's as scattering orbitals. In SEP calculations, the two C_{3v} molecules were treated as belonging to C_s. For each of these systems, only the A' IR of C_s was polarized;

TABLE II. Calculated and experimental [36] permanent electric dipole moments (Debye) and static electric polarizabilities (10^{-24} cm^3) for fluoromethanes.

System	D^{calc}	D^{expt}	$\alpha_{xx}^{\text{calc}}$	$\alpha_{yy}^{\text{calc}}$	$\alpha_{zz}^{\text{calc}}$	$\alpha_{\text{aver}}^{\text{calc}}$	$\alpha_{\text{aver}}^{\text{expt}}$
CH_3F	2.103	1.858	2.507	2.507	2.511	2.508	2.97
CH_2F_2	2.177	1.978	2.559	2.409	2.308	2.425	
CHF_3	1.833	1.651	2.655	2.655	2.494	2.601	3.54
CF_4			2.764	2.764	2.764	2.764	3.838

that is, only configurations of overall $^2A'$ symmetry were considered in addition to the SE configurations. In terms of C_{3v}, this amounts to polarizing the A_1 IR and one component of the doubly degenerate E IR. To obtain a balanced description of the E IR, we employed an angular momentum decomposition of the SMC scattering amplitude [39] to generate the remaining E component via rotation. As a result, we obtained polarized descriptions of the A_1 and E representations of the C_{3v} group, while the A_2 IR remained described at the SE level, an acceptable approximation due to its very modest contribution to low-energy cross sections. For CF_4, each IR of C_{2v} was polarized, with B_2 being generated from B_1 through angular momentum decomposition and rotation. For CH_2F_2, each IR of C_{2v} was polarized except A_2, whose SE partial cross section was found to be very small at the energies considered. Not all possible single excitations were included, in order to reduce the computational effort. Excitations with small dipole transition moments and those out of valence orbitals with less significant contributions to the polarizabilities of the targets were dropped. The configuration spaces are summarized in Table I.

In obtaining rotationally resolved scattering amplitudes, as well as in generating the second E component of C_{3v} molecules and the B_2 IR of CF_4, partial-wave expansions were carried out up to $\ell = 10$. We have used experimental dipole moment magnitudes in Born corrections, since the calculated values are about 10% too large (see Table II).

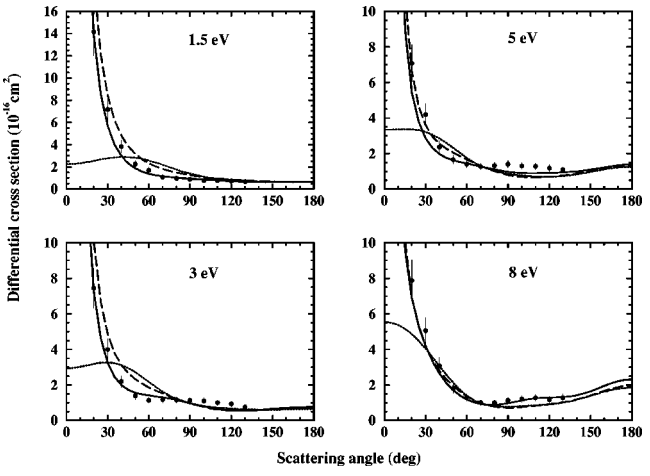

FIG. 1. Elastic differential cross section for e^--CH_3F scattering at 1.5, 3, 5, and 8 eV. Dotted line, present SE calculation without Born closure; dashed line, present SE calculation with Born closure; solid line, present SEP calculation with Born closure; bullets, present experimental result.

These calculated dipole moment magnitudes were obtained through restricted Hartree-Fock (RHF) calculations using the basis sets described above, while static-electric polarizabilities, also shown in Table II, were calculated within a single-excitation configuration-interaction framework with the same basis sets.

IV. EXPERIMENT

The experimental procedures and the details of the apparatus used in the present measurements have been previously described [40]. Briefly, electrons from a hemispherical monochromator cross an effusive molecular beam at right angles, and scattered electrons are energy analyzed in a second hemispherical system, detected by a channeltron electron multiplier, and stored in a multichannel analyzer utilizing pulse-counting techniques. A number of tube lenses, whose characteristics were carefully confirmed by electron trajectory calculations, have been used for imaging and energy control of the electron beam in the spectrometer. To keep the transmission of the electrons constant in the lens system, programmable power supplies are used to control the driving voltages of some lens elements, guided by the trajectory calculations. Both the monochromator and the analyzer are enclosed in differentially pumped boxes to reduce the effect of the background gases and to minimize the stray electron background. The target molecular beam is produced by effusing CH_xF_{4-x} through a simple nozzle with an internal diameter of 0.3 mm and a length of 5 mm. The spectrometer and the nozzle are heated to a temperature of about 50 °C to reduce any possibility of contamination during the

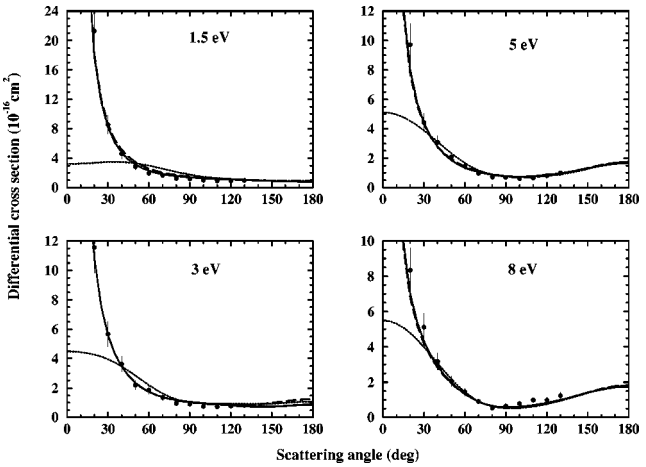

FIG. 2. As in Fig. 1, but for CH_2F_2.

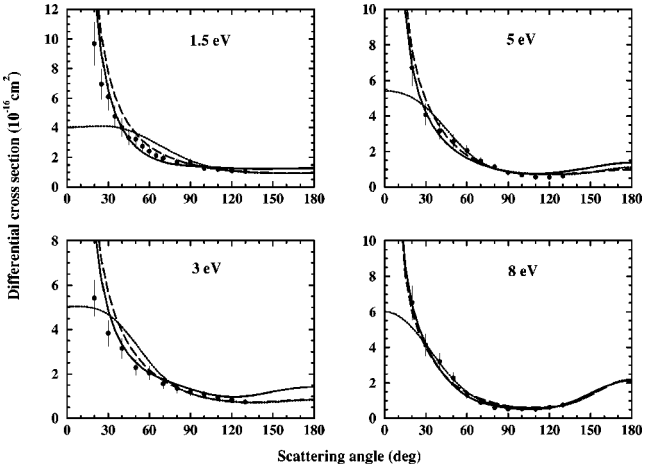

FIG. 3. As in Fig. 1, but for CHF_3.

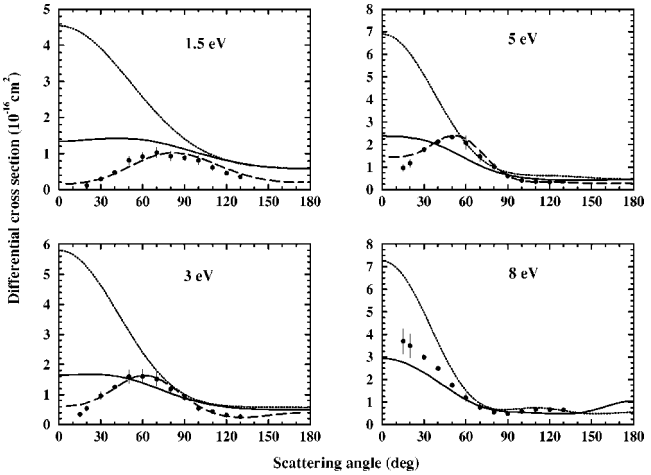

FIG. 4. Elastic differential cross section for e^--CF_4 scattering at 1.5, 3, 5, and 8 eV. Dotted line, present SE calculation; solid line, present SEP calculation; long-dashed line, CKM calculation of Ref. [15]; bullets, experimental results of Ref. [21].

measurements. The analyzer can be rotated around the scattering center, covering an angular range from $-10°$ to 130° with respect to the incident electron beam. Actually, the DCS measurements are limited due to the parent incident electron beam at the forward-scattering angles, i.e., down to 20° for incident energies less than 5 eV and 15° for higher energies. The overall energy resolution of the present measurements was 35–40 meV, and the angular resolution was $\pm 15°$. This energy resolution is, however, not sufficient to resolve any rotational excitations.

Absolute cross sections were obtained by the relative flow technique [41] using helium as the comparison gas. So that the densities of the two gases can be assumed to be identical, the pressure behind the nozzle is adjusted to maintain approximately equal gas Knudsen numbers. In this connection, based on gas-kinetic calculations, the pressures were estimated by using a hard-sphere diameter of 2.19 Å for helium along with corresponding diameters of 4.68, 4.91, and 4.95 Å for CH_3F, CH_2F_2, and CHF_3 (estimated from the critical constants T_c, P_c, and V_c [42]), respectively. The gases were purchased from Takachiho Chemicals Co. Ltd.

TABLE III. Experimental and calculated (dipole-corrected SEP approximation) elastic differential cross sections (10^{-16} cm^2 sr^{-1}) for fluoromethanes at 1.5 eV.

Angle (deg)	CH_3F		CH_2F_2		CHF_3		CF_4	
	Calc.	Expt.	Calc.	Expt.	Calc.	Expt.	Calc.	Expt.
0.0							1.338	
10.0	58.40		68.60		48.79		1.350	
15.0	25.38		31.06		22.62		1.363	
20.0	13.85	14.15	17.83	21.33	13.36	9.687	1.378	0.116
30.0	5.699	7.187	8.225	8.564	6.549	6.090	1.407	0.293
40.0	2.979	3.836	4.772	4.607	3.990	4.025	1.422	0.475
50.0	1.860	2.252	3.145	2.837	2.733	3.238	1.416	0.811
60.0	1.370	1.690	2.285	1.959	2.059	2.426	1.382	0.915
70.0	1.148	1.071	1.820	1.646	1.701	1.936	1.318	1.026
80.0	1.032	0.957	1.559	1.256	1.521	1.676	1.228	0.922
90.0	0.946	0.882	1.392	1.186	1.428	1.660	1.123	0.878
100.0	0.866	0.766	1.277	0.983	1.371	1.277	1.013	0.815
110.0	0.789	0.770	1.192	0.946	1.322	1.192	0.907	0.615
120.0	0.722	0.720	1.115	0.944	1.277	1.093	0.812	0.458
130.0	0.672	0.670	1.036	0.964	1.243	1.052	0.733	0.362
140.0	0.639		0.969		1.228		0.670	
150.0	0.621		0.909		1.233		0.624	
160.0	0.614		0.851		1.251		0.595	
170.0	0.612		0.816		1.269		0.580	
180.0	0.612		0.810		1.277		0.576	

TABLE IV. As in Table III but at 2 eV.

	CH_3F		CH_2F_2		CHF_3		CF_4	
Angle (deg)	Calc.	Expt.	Calc.	Expt.	Calc.	Expt.	Calc.	Expt.
0.0							1.451	
10.0	44.29		52.76		37.84		1.462	
15.0	19.52		24.52		18.16		1.474	0.119
20.0	10.86	9.828	14.49	16.28	11.15	7.502	1.488	0.211
30.0	4.735	5.656	7.071	6.856	5.891	4.810	1.508	0.517
40.0	2.690	3.121	4.275	4.160	3.832	3.273	1.507	0.753
50.0	1.851	2.113	2.882	2.505	2.784	2.411	1.475	1.118
60.0	1.469	1.409	2.112	1.714	2.205	2.115	1.406	1.399
70.0	1.261	1.068	1.679	1.298	1.876	1.831	1.303	1.258
80.0	1.103	1.048	1.425	1.082	1.673	1.582	1.178	1.044
90.0	0.953	0.832	1.256	1.064	1.523	1.424	1.045	0.806
100.0	0.812	0.892	1.134	0.934	1.388	1.211	0.919	0.726
110.0	0.695	0.858	1.043	0.945	1.267	1.097	0.807	0.486
120.0	0.614	0.766	0.958	0.856	1.174	1.008	0.716	0.403
130.0	0.572	0.698	0.877	0.874	1.125	0.964	0.646	0.298
140.0	0.562		0.814		1.126		0.594	
150.0	0.572		0.771		1.168		0.558	
160.0	0.591		0.745		1.227		0.538	
170.0	0.607		0.746		1.277		0.528	
180.0	0.613		0.755		1.296		0.526	

TABLE V. As in Table III but at 3 eV.

	CH_3F		CH_2F_2		CHF_3		CF_4	
Angle (deg)	Calc.	Expt.	Calc.	Expt.	Calc.	Expt.	Calc.	Expt.
0.0							1.649	
10.0	29.51		36.69		26.53		1.656	
15.0	13.01		17.72		13.33		1.663	0.341
20.0	7.260	7.444	10.877	11.56	8.574	5.425	1.669	0.544
30.0	3.244	4.002	5.597	5.668	4.874	3.839	1.664	0.957
40.0	1.995	2.188	3.463	3.613	3.340	3.152	1.619	1.256
50.0	1.565	1.379	2.348	2.208	2.529	2.294	1.525	1.591
60.0	1.410	1.145	1.727	1.854	2.061	2.053	1.386	1.603
70.0	1.300	1.163	1.388	1.351	1.759	1.560	1.216	1.513
80.0	1.153	1.155	1.191	0.956	1.526	1.350	1.041	1.179
90.0	0.968	1.121	1.057	0.905	1.321	1.184	0.883	0.891
100.0	0.785	1.098	0.961	0.747	1.146	1.081	0.754	0.538
110.0	0.645	1.000	0.889	0.719	1.023	0.924	0.657	0.440
120.0	0.568	0.929	0.822	0.773	0.974	0.860	0.590	0.317
130.0	0.554	0.764	0.761	0.833	1.003	0.744	0.545	0.264
140.0	0.586		0.729		1.092		0.516	
150.0	0.642		0.735		1.207		0.500	
160.0	0.702		0.776		1.315		0.493	
170.0	0.746		0.845		1.390		0.494	
180.0	0.762		0.883		1.416		0.495	

TABLE VI. As in Table III but at 5 eV.

	CH_3F		CH_2F_2		CHF_3		CF_4	
Angle (deg)	Calc.	Expt.	Calc.	Expt.	Calc.	Expt.	Calc.	Expt.
0.0							2.373	
10.0	18.96		23.94		17.93		2.360	
15.0	8.99		12.37		9.863		2.340	0.965
20.0	5.44	7.084	8.027	9.721	6.825	6.715	2.307	1.178
30.0	2.854	4.198	4.400	4.418	4.198	4.082	2.186	1.778
40.0	1.973	2.367	2.759	3.082	2.905	3.159	1.979	2.131
50.0	1.622	1.647	1.858	2.083	2.129	2.579	1.696	2.334
60.0	1.438	1.404	1.349	1.452	1.633	2.062	1.375	2.081
70.0	1.272	1.262	1.059	0.973	1.290	1.451	1.069	1.472
80.0	1.105	1.310	0.884	0.725	1.037	1.138	0.822	1.023
90.0	0.973	1.406	0.781	0.683	0.858	0.828	0.651	0.607
100.0	0.907	1.302	0.747	0.616	0.759	0.673	0.544	0.408
110.0	0.895	1.282	0.781	0.649	0.741	0.556	0.482	0.355
120.0	0.910	1.186	0.863	0.821	0.785	0.541	0.445	0.336
130.0	0.939	1.081	0.980	0.983	0.869	0.630	0.423	0.378
140.0	0.995		1.134		0.978		0.414	
150.0	1.094		1.309		1.104		0.417	
160.0	1.224		1.479		1.236		0.431	
170.0	1.339		1.623		1.343		0.449	
180.0	1.385		1.686		1.384		0.457	

TABLE VII. As in Table III but at 6.5 eV.

	CH_3F		CH_2F_2		CHF_3		CF_4 [a]	
Angle (deg)	Calc.	Expt.	Calc.	Expt.	Calc.	Expt.	Calc.	Expt.
0.0							2.507	
10.0	16.88		20.09		15.20		2.486	
15.0	9.014		11.03		8.881		2.457	1.553
20.0	6.039	7.790	7.513	8.876	6.397	6.442	2.411	1.674
30.0	3.488	4.479	4.352	4.471	4.051	4.660	2.346	2.041
40.0	2.306	2.936	2.789	2.807	2.766	3.311	2.256	2.363
50.0	1.673	1.806	1.878	2.062	1.959	2.444	2.004	2.418
60.0	1.323	1.246	1.327	1.363	1.446	1.784	1.671	1.938
70.0	1.121	1.111	0.983	0.867	1.107	1.239	1.309	1.484
80.0	1.017	1.228	0.760	0.616	0.874	0.884	0.982	0.903
90.0	0.998	1.407	0.633	0.644	0.721	0.577	0.739	0.543
100.0	1.036	1.338	0.603	0.613	0.642	0.488	0.587	0.377
110.0	1.084	1.200	0.663	0.742	0.631	0.527	0.504	0.435
120.0	1.118	1.185	0.795	0.990	0.681	0.544	0.456	0.447
130.0	1.160	1.121	0.981	1.086	0.792	0.772	0.426	0.450
140.0	1.265		1.208		0.972		0.407	
150.0	1.462		1.443		1.217		0.405	
160.0	1.718		1.650		1.491		0.425	
170.0	1.939		1.806		1.714		0.463	
180.0	2.027		1.868		1.801		0.503	

[a]6.0 eV.

TABLE VIII. As in Table III but at 7 eV.

	CH_3F		CH_2F_2		CHF_3		CF_4	
Angle (deg)	Calc.	Expt.	Calc.	Expt.	Calc.	Expt.	Calc.	Expt.
0.0							2.540	
10.0	16.58		18.56		14.67		2.510	
15.0	9.196		10.19		8.755		2.472	2.557
20.0	6.333	8.099	6.972	8.482	6.385	6.484	2.416	2.472
30.0	3.737	4.652	4.142	4.913	4.071	4.495	2.239	2.378
40.0	2.430	2.849	2.760	3.526	2.760	3.155	1.966	2.422
50.0	1.688	1.718	1.914	2.175	1.932	2.173	1.612	2.052
60.0	1.274	1.370	1.347	1.395	1.411	1.549	1.232	1.780
70.0	1.055	1.156	0.963	0.889	1.077	1.004	0.902	1.109
80.0	0.973	1.143	0.721	0.622	0.851	0.681	0.676	0.657
90.0	0.995	1.278	0.605	0.643	0.699	0.567	0.554	0.435
100.0	1.072	1.288	0.596	0.659	0.613	0.471	0.497	0.468
110.0	1.142	1.315	0.671	0.814	0.590	0.531	0.464	0.538
120.0	1.179	1.242	0.810	0.931	0.635	0.605	0.433	0.593
130.0	1.219	1.240	1.002	1.045	0.760	0.737	0.414	0.574
140.0	1.328		1.232		0.972		0.425	
150.0	1.543		1.465		1.265		0.480	
160.0	1.825		1.660		1.589		0.569	
170.0	2.069		1.798		1.851		0.657	
180.0	2.165		1.852		1.953		0.694	

TABLE IX. As in Table III but at 8 eV.

	CH_3F		CH_2F_2		CHF_3		CF_4	
Angle (deg)	Calc.	Expt.	Calc.	Expt.	Calc.	Expt.	Calc.	Expt.
0.0							2.942	
10.0	16.23		17.39		13.84		2.860	
15.0	9.606		9.966		8.592		2.763	3.704
20.0	6.903	7.891	7.034	8.349	6.421	6.511	2.635	3.506
30.0	4.193	5.052	4.320	5.122	4.164	4.129	2.304	2.987
40.0	2.651	3.076	2.896	3.171	2.779	3.199	1.907	2.489
50.0	1.712	1.800	1.970	2.062	1.854	2.277	1.490	1.757
60.0	1.175	1.292	1.324	1.437	1.264	1.341	1.110	1.197
70.0	0.918	1.005	0.891	0.904	0.909	0.901	0.822	0.775
80.0	0.870	1.001	0.650	0.538	0.704	0.603	0.650	0.552
90.0	0.969	1.123	0.571	0.635	0.589	0.536	0.576	0.495
100.0	1.124	1.202	0.604	0.788	0.529	0.530	0.549	0.592
110.0	1.241	1.272	0.696	0.984	0.522	0.524	0.527	0.678
120.0	1.289	1.160	0.824	0.986	0.592	0.624	0.495	0.670
130.0	1.318	1.286	0.989	1.238	0.767	0.756	0.477	0.662
140.0	1.419		1.189		1.052		0.513	
150.0	1.642		1.397		1.410		0.628	
160.0	1.945		1.574		1.768		0.803	
170.0	2.210		1.700		2.034		0.973	
180.0	2.316		1.748		2.132		1.045	

TABLE X. As in Table III but at 9 eV.

	CH_3F		CH_2F_2		CHF_3		CF_4	
Angle (deg)	Calc.	Expt.	Calc.	Expt.	Calc.	Expt.	Calc.	Expt.
0.0							3.711	
10.0	16.67		15.86		13.81		3.541	
15.0	10.55		9.240		9.003		3.348	4.715
20.0	7.859	8.349	6.604	8.139	6.898	6.587	3.107	4.097
30.0	4.838	5.052	4.128	4.920	4.509	4.774	2.559	3.513
40.0	2.956	2.992	2.807	2.934	2.947	3.203	2.015	2.656
50.0	1.784	1.814	1.940	1.964	1.906	2.254	1.530	1.714
60.0	1.132	1.111	1.334	1.377	1.274	1.434	1.133	1.115
70.0	0.848	0.896	0.937	0.768	0.922	0.899	0.858	0.720
80.0	0.828	0.889	0.733	0.660	0.728	0.630	0.727	0.605
90.0	0.970	0.900	0.687	0.753	0.611	0.633	0.712	0.681
100.0	1.143	1.063	0.737	0.847	0.537	0.581	0.737	0.767
110.0	1.241	1.112	0.820	1.016	0.527	0.615	0.723	0.754
120.0	1.244	1.233	0.910	1.099	0.629	0.662	0.650	0.731
130.0	1.229	1.184	1.016	1.209	0.878	0.821	0.578	0.658
140.0	1.307		1.154		1.264		0.611	
150.0	1.533		1.327		1.726		0.816	
160.0	1.853		1.531		2.168		1.159	
170.0	2.137		1.728		2.486		1.496	
180.0	2.250		1.816		2.601		1.639	

TABLE XI. As in Table III but at 10 eV.

	CH_3F		CH_2F_2		CHF_3		CF_4	
Angle (deg)	Calc.	Expt.	Calc.	Expt.	Calc.	Expt.	Calc.	Expt.
0.0							5.433	
10.0	16.18		15.30		13.37		5.070	
15.0	10.57	9.992	9.225	13.09	8.874	0.000	4.660	4.401
20.0	8.015	8.262	6.721	10.04	6.791	7.309	4.158	4.768
30.0	4.990	5.194	4.232	5.047	4.290	4.716	3.083	4.116
40.0	2.993	3.305	2.836	2.885	2.688	3.231	2.167	2.884
50.0	1.704	1.820	1.913	1.913	1.726	2.130	1.533	1.685
60.0	0.983	1.077	1.277	1.252	1.224	1.365	1.154	0.999
70.0	0.694	0.811	0.880	0.765	0.977	0.856	0.963	0.730
80.0	0.719	0.772	0.703	0.769	0.840	0.659	0.911	0.782
90.0	0.926	0.943	0.698	0.756	0.743	0.638	0.940	0.800
100.0	1.158	1.012	0.780	0.809	0.672	0.681	0.968	0.794
110.0	1.287	1.056	0.869	1.032	0.660	0.701	0.924	0.727
120.0	1.290	1.047	0.936	1.103	0.758	0.751	0.800	0.622
130.0	1.255	1.170	0.999	1.093	1.002	0.850	0.684	0.651
140.0	1.308		1.086		1.383		0.718	
150.0	1.517		1.212		1.839		0.990	
160.0	1.832		1.378		2.280		1.448	
170.0	2.118		1.550		2.602		1.895	
180.0	2.232		1.629		2.721		2.082	

TABLE XII. As in Table III but at 15 eV.

	CH_3F		CH_2F_2		CHF_3		CF_4	
Angle (deg)	Calc.	Expt.	Calc.	Expt.	Calc.	Expt.	Calc.	Expt.
0.0							6.256	
10.0	14.691		15.507		13.591		5.783	
15.0	10.448	9.741	10.624	11.872	10.017	8.455	5.242	5.433
20.0	8.152	8.584	7.996	9.232	7.933	6.287	4.569	4.822
30.0	4.963	4.773	4.576	4.549	4.852	4.275	3.097	3.473
40.0	2.796	2.544	2.568	2.320	2.735	2.683	1.862	2.464
50.0	1.498	1.501	1.541	1.470	1.547	1.619	1.128	1.383
60.0	0.834	0.934	1.054	0.987	1.022	1.030	0.866	0.901
70.0	0.576	0.660	0.833	0.700	0.821	0.753	0.855	0.869
80.0	0.573	0.626	0.784	0.756	0.729	0.800	0.863	1.058
90.0	0.702	0.614	0.841	0.716	0.678	0.754	0.778	1.076
100.0	0.834	0.638	0.912	0.818	0.675	0.763	0.636	0.931
110.0	0.887	0.639	0.935	0.712	0.729	0.791	0.529	0.698
120.0	0.877	0.674	0.926	0.830	0.822	0.751	0.517	0.595
130.0	0.901	0.757	0.944	0.845	0.926	0.863	0.596	0.691
140.0	1.062		1.032		1.032		0.735	
150.0	1.382		1.197		1.153		0.906	
160.0	1.779		1.413		1.295		1.090	
170.0	2.106		1.618		1.421		1.244	
180.0	2.232		1.707		1.473		1.306	

The electron energy scale was calibrated with respect to the 19.367 eV resonance in He. Experimental errors are estimated to be 15–20% for the elastic DCS's due to a combination of statistical, systematic and normalization errors in the experiments.

V. RESULTS

Figures 1 to 4 show elastic differential cross sections (DCS) for CH_3F, CH_2F_2, CHF_3, and CF_4, at 1.5, 3, 5, and 8 eV. The experimental and SEP DCS at various energies are also presented in Tables III–XIV. As mentioned in the Introduction, the measured values for CF_4 are taken from earlier work [28] and included here for ease of comparison. For the polar systems (Figs. 1 to 3), the present theoretical results are shown at three levels of approximation: (i) SE approximation without Born closure, (ii) SE approximation with Born closure, and (iii) SEP approximation with Born closure. For CF_4, we show SE and SEP calculations. Although not shown here, previous SE calculations by Natalense *et al.* [18] are in good agreement with the present SE results for CH_3F, CH_2F_2, and CHF_3 beyond 5 eV. The present SE DCS of CF_4 also agrees with earlier SMC [43] and SMCPP (SMC with pseudopotentials) [16,44] calculations. As expected, dipole-Born corrections are essential to describe the DCS of polar molecules at small scattering angles ($\theta<30°$). For CH_2F_2, the system with the largest dipole moment and the smallest calculated polarizability (see Table II), the dipole-corrected SE and SEP calculations are always very close to each other and fairly close to the experimental values. For CF_4, on the other hand, one observes that only at 8 eV do the SEP calculations describe the measured DCS reasonably well, although inclusion of polarization effects always significantly improves the SE results. Figure 4 also shows the results of the calculations of Isaacs *et al.* [15] employing the complex Kohn method (CKM), which agree very well with present and previously reported [45,46] experimental results. We believe that our results for CF_4 could be improved by augmenting the configuration space. The *ab initio* CKM calculation included about 19 000 configurations per irreducible representation of C_{2v}, while the present calculations only include about 3000 (see Table I).

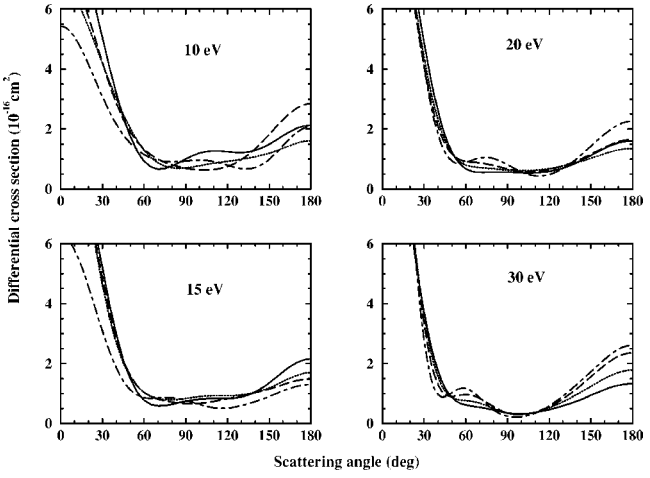

FIG. 5. Elastic differential cross section for electron collisions with fluoromethanes at 10, 15, 20, and 30 eV. Solid line, CH_3F; dotted line, CH_2F_2; dashed line, CHF_3; dot-dashed line, CF_4.

TABLE XIII. As in Table III but at 20 eV.

	CH_3F		CH_2F_2		CHF_3		CF_4	
Angle (deg)	Calc.	Expt.	Calc.	Expt.	Calc.	Expt.	Calc.	Expt.
0.0							11.80	
10.0	14.69		14.02		12.54		10.52	
15.0	10.45	10.36	9.710		9.372	9.500	9.100	6.757
20.0	8.071	7.673	7.415	9.098	7.260	7.214	7.412	5.146
30.0	4.726	4.141	4.271	4.629	4.008	3.804	4.084	3.167
40.0	2.501	2.134	2.240	2.061	1.996	2.090	1.830	1.720
50.0	1.235	1.183	1.200	1.264	1.134	1.122	0.936	0.912
60.0	0.679	0.744	0.815	1.000	0.922	0.782	0.892	0.795
70.0	0.541	0.641	0.714	0.835	0.878	0.855	1.041	1.004
80.0	0.561	0.580	0.686	0.745	0.793	0.836	1.021	1.095
90.0	0.579	0.516	0.653	0.677	0.673	0.732	0.816	0.988
100.0	0.562	0.398	0.616	0.540	0.590	0.567	0.576	0.690
110.0	0.550	0.429	0.630	0.580	0.583	0.530	0.446	0.530
120.0	0.588	0.440	0.711	0.662	0.650	0.585	0.487	0.554
130.0	0.697	0.573	0.805	0.738	0.777	0.762	0.690	0.823
140.0	0.879		0.896		0.956		1.020	
150.0	1.118		1.027		1.176		1.426	
160.0	1.362		1.196		1.406		1.837	
170.0	1.544		1.330		1.586		2.150	
180.0	1.611		1.377		1.655		2.268	

TABLE XIV. As in Table III but at 30 eV.

	CH_3F		CH_2F_2		CHF_3		CF_4 [a]	
Angle (deg)	Calc.	Expt.	Calc.	Expt.	Calc.	Expt.	Calc.	Expt.
0.0							16.79	
10.0	12.36		13.66		14.19		13.92	
15.0	8.941	10.20	9.823	12.21	10.49	12.14	10.96	14.10
20.0	6.727	7.924	7.251	7.567	7.606	8.678	7.759	7.827
30.0	3.545	3.167	3.526	2.877	3.284	3.465	2.792	2.691
40.0	1.697	1.370	1.550	1.387	1.279	1.154	0.968	0.878
50.0	0.863	0.613	0.883	0.687	0.912	0.795	1.030	0.861
60.0	0.601	0.498	0.754	0.654	0.966	0.749	1.171	0.927
70.0	0.533	0.475	0.669	0.649	0.831	0.768	0.861	0.809
80.0	0.455	0.344	0.514	0.427	0.558	0.578	0.456	0.435
90.0	0.361	0.233	0.362	0.260	0.352	0.321	0.245	0.201
100.0	0.323	0.187	0.307	0.194	0.297	0.222	0.229	0.176
110.0	0.360	0.200	0.381	0.255	0.374	0.287	0.348	0.255
120.0	0.448	0.295	0.545	0.328	0.556	0.453	0.587	0.455
130.0	0.572	0.397	0.736	0.592	0.829	0.631	0.921	0.691
140.0	0.734		0.938		1.176		1.311	
150.0	0.929		1.179		1.567		1.728	
160.0	1.123		1.452		1.946		2.145	
170.0	1.264		1.680		2.232		2.482	
180.0	1.315		1.769		2.339		2.615	

[a]35 eV.

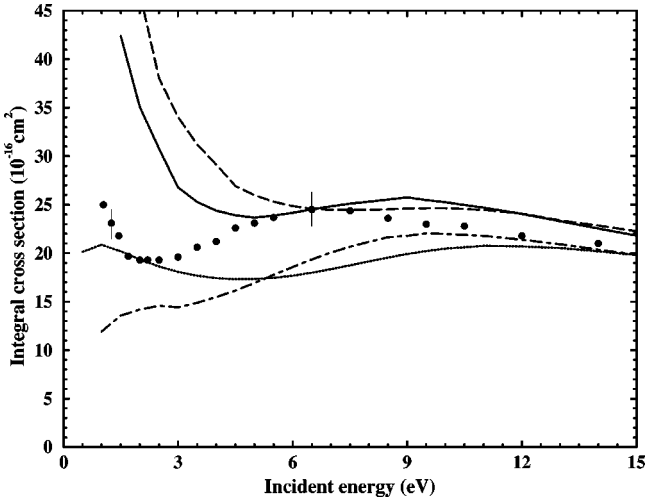

FIG. 6. Elastic integral cross section for e^--CH_3F scattering. Dotted line, present SE calculation (without Born closure); dot-dashed line, present SEP calculation (without Born closure); dashed line, present SE calculation (Born corrected); solid line, present SEP calculation (Born corrected); bullets, experimental total cross section of Ref. [6].

Figure 5 shows Born-corrected calculated DCS at 10, 15, 20, and 30 eV. Polarization effects are not included in results beyond 15 eV. It has been previously observed [17] that replacement of H by F causes a bump in the DCS around 60–65° at impact energies in the range 20–30 eV. This structure was found to become more pronounced as more H atoms were replaced (the so-called *fluorination effect*). That effect is also visible here. CF_4 already shows a slight bump at 15 eV, which becomes very pronounced at 20 and 30 eV. A similar but less prominent structure appears in the CHF_3 and CH_2F_2 DCS at 20 and 30 eV, while for CH_3F, only a slight undulation at 30 eV is seen. Measured and calculated (dipole-corrected SE) DCS at 20 and 30 eV (35 eV for CF_4) are shown, respectively, in Tables XIII and XIV. At 60° and 30 eV, one finds, as expected, that the differential cross section increases with the number of F atoms in the molecule, i.e., $\sigma_{CH_3F}<\sigma_{CH_2F_2}<\sigma_{CHF_3}<\sigma_{CF_4}$.

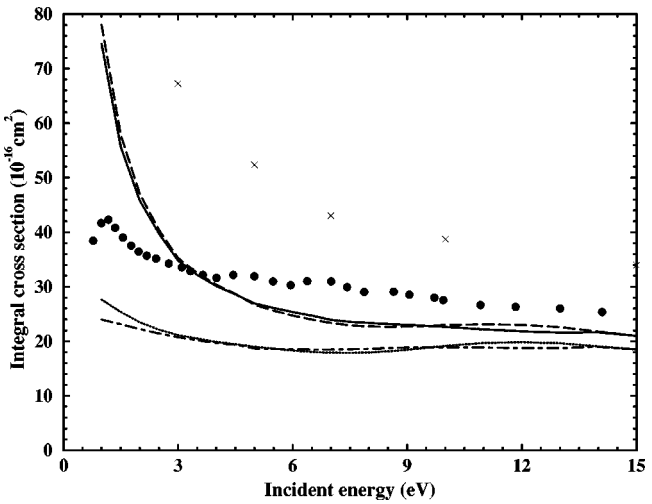

FIG. 7. Elastic integral cross section for e^--CH_2F_2 scattering. Dotted line, present SE calculation (without Born closure); dot-dashed line, present SEP calculation (without Born closure); dashed line, present SE calculation (Born corrected); solid line, present SEP calculation (Born corrected); crosses, calculation of Ref. [8]; bullets, experimental total cross section of Ref. [7].

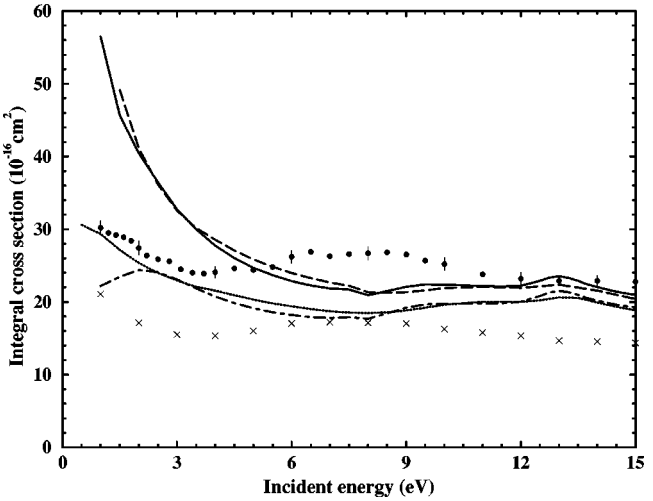

FIG. 8. Elastic integral cross section for e^--CHF_3 scattering. Dotted line, present SE calculation (without Born closure); dot-dashed line, present SEP calculation (without Born closure); dashed line, present SE calculation (Born corrected); solid line, present SEP calculation (Born corrected); bullets, experimental total cross section of Ref. [10]; crosses, experimental total cross section of Ref. [11].

Figures 6 to 9 show calculated integral cross sections (ICS) for CH_3F, CH_2F_2, CHF_3, and CF_4. For CH_3F (Fig. 6) one observes an overall agreement in shape with the experimental total cross section (TCS) of Krzysztofowicz and Szmytkowski [6], although the broad structure seen in the

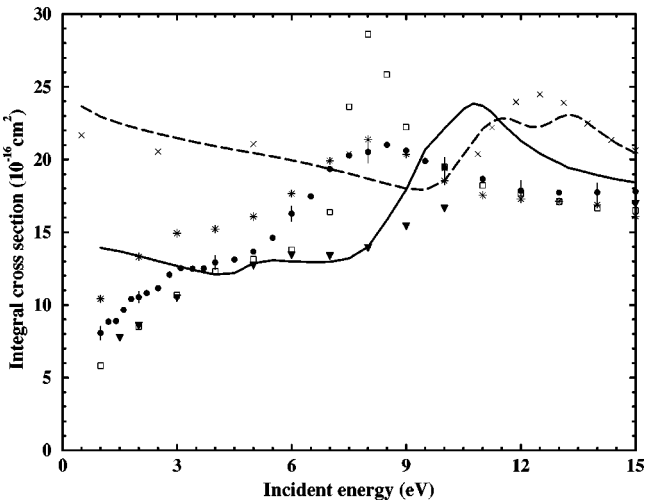

FIG. 9. Elastic integral cross section for e^--CF_4 scattering. Dashed line, present SE calculation; solid line, present SEP calculation; crosses, SE calculation of Ref. [15]; open squares, SEP calculation of Ref. [15]; triangles, experimental elastic cross section of Ref. [45]; bullets, experimental total cross section of Ref. [47].

TABLE XV. Calculated elastic integral cross sections (10^{-16} cm^2) for fluoromethanes.

Energy (eV)	CH_3F	CH_2F_2	CHF_3	CF_4
1.5	42.38	55.65	45.62	13.69
2	35.08	45.79	40.46	13.36
3	26.78	34.82	32.75	12.68
4	24.37	30.16	27.76	12.09
5	23.67	26.97	24.70	12.87
6	24.17	25.37	22.88	12.99
7	24.84	23.92	21.85	12.95
8	25.32	23.36	20.94	14.00
9	25.76	23.04	22.09	17.94
10	25.24	22.61	22.38	22.12
11	24.71	22.21	22.21	23.69
12	24.04	21.84	22.23	21.30
13	23.30	21.58	23.52	19.76
14	22.55	21.62	22.03	18.92
15	21.80	21.00	20.96	18.42

ICS (5–10 eV) is shifted to the right relative to experiment. However, the calculated elastic ICS is generally larger than the measured TCS, especially below 5 eV but even at higher energies ($E>11$ eV) where open inelastic electronic channels are found. The present calculated ICS of CH_2F_2, (Fig. 7), does not agree with the calculations of Nishimura [8]. This was to be expected because Nishimura's DCS was too large in comparison with the present experimental and calculated data. The calculated ICS is also larger than the experimental TCS of Kimura *et al.* [7] below 3 eV. The agreement between the SE and SEP calculations for this molecule, already seen in the DCS, is of course preserved in the ICS. The dipole-corrected ICS of CHF_3 (Fig. 8) once again exceeds the experimental TCS at low impact energies; although considerable discrepancy exists between the TCS measurements of Sueoka *et al.* [10] and those of Sanabia *et al.* [11], the calculated ICS is larger than either TCS below about 5 eV. The experimental data show a broad maximum between 5 and 10 eV not observed in the calculations, while the calculated cross sections show a structure around 13 eV not found experimentally. Since inelastic electronic channels are open at 13 eV, the inelastic contribution to the TCS may be masking the structure in the elastic channel. Finally, the calculated ICS of CF_4 is shown in Fig. 9 along with the SE and SEP calculations of Isaacs *et al.* [15], obtained with the complex Kohn method (CKM), and of Gianturco *et al.* [14], obtained from a potential-scattering calculation. The experimental elastic ICS of Boesten *et al.* [45] and the TCS of Sueoka *et al.* [47] are also shown for comparison purposes. Though not shown here, TCS measurements of Szmytkowski *et al.* [48] and of Jones [49] agree very well with those of Sueoka *et al.* It should be observed that our SE ICS agrees

TABLE XVI. Calculated elastic momentum-transfer cross sections (10^{-16} cm^2) for fluoromethanes.

Energy (eV)	CH_3F	CH_2F_2	CHF_3	CF_4
1.5	11.62	17.56	18.79	11.52
2	10.93	15.48	18.50	10.70
3	10.60	13.27	16.68	9.442
4	11.63	12.80	14.50	8.444
5	13.58	13.70	13.26	7.893
6	15.18	13.51	12.70	7.571
7	16.36	13.35	12.42	7.607
8	17.05	13.06	12.17	8.349
9	16.58	13.61	13.59	10.32
10	16.40	13.28	14.84	12.53
11	15.80	12.99	14.39	14.29
12	15.12	12.73	14.01	11.91
13	14.44	12.56	14.43	10.64
14	13.81	12.68	13.79	10.09
15	13.25	11.96	13.08	9.850

TABLE XVII. Relative standard deviation from experimental data for fluoromethanes in different approximations: static-exchange (SE); Born-corrected SE (B-SE); static-exchange–plus–polarization (SEP); Born-corrected SEP (B-SEP).

System	Energy (eV)	Approx.	Δ
CH_3F	1.5	SE	0.563
		B-SE	0.379
		B-SEP	0.127
CH_2F_2	1.5	SE	0.488
		B-SE	0.255
		B-SEP	0.174
CHF_3	1.5	SE	0.272
		B-SE	0.228
		B-SEP	0.162
CF_4	1.5	SE	11.13
		SEP	3.427
CH_3F	5	SE	0.349
		B-SE	0.303
		B-SEP	0.216
CH_2F_2	5	SE	0.204
		B-SE	0.122
		B-SEP	0.137
CHF_3	5	SE	0.220
		B-SE	0.177
		B-SEP	0.182
CF_4	5	SE	2.059
		SEP	0.531
CH_3F	8	SE	0.240
		B-SE	0.203
		B-SEP	0.106
CH_2F_2	8	SE	0.229
		B-SE	0.167
		B-SEP	0.165
CHF_3	8	SE	0.154
		B-SE	0.190
		B-SEP	0.090
CF_4	8	SE	0.427
		SEP	0.201

TABLE XVIII. Resonance positions for fluoromethanes (eV).

System	Symmetry	IR	Present	Ref. [51] (calc.)	Ref. [51] (expt.)
CH_3F	C_{3v}	A_1	9.5[a]	10.12	
CH_2F_2	C_{2v}	A_1	10.5[a]	10.17	
		B_2	11.5	9.44	
CHF_3	C_{3v}	A_1	9.3 and 13.0	9.64	
		E	10.8	9.44	
					9.3
CF_4	T_d	A_1	11.0	8.58	
		T_2	9.9	8.98	
					7.9

[a]These assignments are less certain.

well with the CKM SE calculation, while one finds some disagreement between the SEP cross sections, attributable to a better representation of polarization in the CKM study. Our result agrees well in both shape and magnitude with the experimental cross sections, but our structures are shifted to higher energy, indicating an insufficient description of polarization effects.

The calculated dipole-corrected SEP integral and momentum-transfer cross sections of the fluoromethanes are given in Tables XV and XVI.

VI. DISCUSSION

A qualitative impression of the agreement between the present measured and calculated differential cross sections may be gained from Figs. 1–5. As a quantitative measure of the agreement between the calculated and measured differential cross sections, it is instructive to consider the relative standard deviation from experimental data $\Delta(E)$ defined as

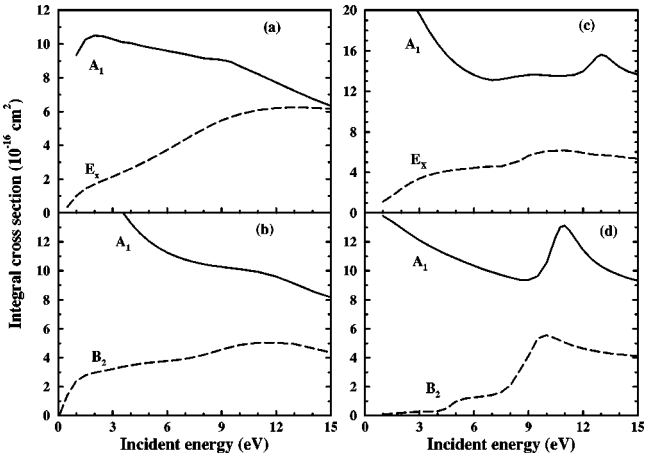

FIG. 10. Partial integral cross sections for the resonant IR of fluoromethanes. (a) CH_3F; (b) CH_2F_2; (c) CHF_3; (d) CF_4.

$$\Delta(E)=\sqrt{\frac{1}{N}\sum_{i=1}^{N}\left[\frac{\sigma^{\mathrm{calc}}(\theta_i)-\sigma^{\mathrm{meas}}(\theta_i)}{\sigma^{\mathrm{meas}}(\theta_i)}\right]^2}, \qquad (14)$$

where $\sigma^{\mathrm{meas}}(\theta_i)$ and $\sigma^{\mathrm{calc}}(\theta_i)$ are, respectively, the measured and calculated DCS at the N scattering angles θ_i for a given impact energy E. Such a relative measure insures that the comparison is not biased toward small angles where the cross section tends to be large and thus allows us to explore the importance of both the longer-range dipole-moment potential and the shorter-range polarization interaction. The size of Δ compared to experimental error ($\sim\pm 15\%$) provides an indication of the agreement between theory and experiment.

Table XVII shows values of Δ at 1.5, 5, and 8 eV for CH_3F, CH_2F_2, CHF_3, and CF_4. For the polar systems, we consider the uncorrected SE, dipole-corrected SE, and dipole-corrected SEP approximations, while SE and SEP results are considered for the nonpolar CF_4. For CH_3F, one finds a deviation above 15% at 5 eV, which is due to a maximum in the experimental DCS at about 80–120° that is not present in the calculated DCS (see Fig. 1). This feature is observed experimentally at impact energies ranging from 3 up to 9 eV but only reproduced in the calculations at 7–9 eV.

For CH_2F_2, we find $\Delta\simeq 0.15$ at all three energies. It is interesting to note, however, that the dipole-corrected SE and SEP results are very close to each other at 5 and 8 eV, indicating that polarization is unimportant above 5 eV for this molecule.

For CHF_3, one again observes significant improvement upon inclusion of polarization at 1.5 and 8 eV. At 5 eV, on the other hand, the dipole-corrected SE and SEP cross sections produce essentially equal deviations ($\Delta\simeq 0.18$). It should be pointed out, however, that SE and SEP calculations at 5 eV (see Fig. 3) are not close to each other at all scattering angles. In fact, the SEP calculation agrees very well with experiment at small angles ($\theta<40°$), while the two curves cross around 90° and the SE values are closer to the measurement above 90°.

At first sight, one could assert that low-energy electron scattering by CH_3F, CH_2F_2, and CHF_3 should be completely dominated by the longest-range interaction, i.e., that between the electron and the dipole moment. Indeed, the absolute correction brought about by the Born-closure procedure, although restricted to small scattering angles ($\theta<30°$), is usually very large. At least for CH_3F and CHF_3, however, the *relative* deviations examined above indicate that polarization is essential to reproducing well the experimental DCS over a broad range of scattering angles.

The comparison between the present calculated ICS and the available experimental TCS of CH_3F, CH_2F_2, and CHF_3 is puzzling (see Figs. 6, 7, and 8). We have no definitive explanation for the fact that experimental TCS is much smaller than the computed elastic ICS at low impact energies ($E<5$ eV). However, it is worth noting that strongly forward-peaked elastic cross sections of polar molecules present a special problem in attenuation measurements, because failure to discriminate between unscattered electrons and electrons elastically scattered in the very-near-forward

direction will lead to an underestimation of the TCS. It is clear from Figs. 1, 2, and 3 that the present calculated and measured DCS are reasonably close at $\theta > 30°$ in all approximations, but that inclusion of the dipolar interaction through Born closure provides a crucial enhancement of the measured cross sections at small scattering angles. We also observe that the same approach used here, i.e., SMC with Born closure and rotational resolution to avoid divergence of the DCS, has led to good agreement with experimental elastic ICS for NH_3 [30], H_2O, H_2S [31], and SO_2 [52].

Considering the ICS of CF_4 (Fig. 9), one sees a double maximum between 10 and 15 eV in the present SE calculation and a single, broader maximum at 10–11 eV in the SEP calculation. As is known from previous calculations, both structures arise from a pair of shape resonances. In the SE approximation, one finds a shape resonance in the A_1 representation (of the full T_d point group) centered at 13.5 eV and another in the T_2 representation at about 11.5 eV, leading to the observed double peak. The A_1 resonance is similar to that observed in CHF_3 at 13 eV, which is visible in Fig. 8. When polarization is included, the resonances shift to lower energy and nearly overlap, the A_1 resonance being centered at 11 eV and the broader T_2 resonance at 10 eV. The overlapping shape resonances are still shifted to higher energy in comparison to the experimental TCS [47,48] and to previous calculations that included polarization effects [14,15]. Our results for CF_4 could be significantly improved by a more effective description of polarization effects, both in the resonance region and below 5 eV, where polarizaton tends to lower the ICS (especially in the totally symmetric A_1 representation). It has been pointed out [28,46] that vibrational excitation significantly contributes to the TCS in the resonant region, and we expect a fixed-nuclei calculation to yield a cross section that is an admixture of the vibrationally elastic and inelastic cross sections, with sharper peaks than in the measured cross sections, under shape-resonant conditions. This is indeed observed when the SEP ICS from the CKM calculation [15] is compared with the experimental TCS. Thus, although the calculations of Gianturco *et al.* [14] agree both in shape and magnitude with the peak in the experimental TCS, it is difficult to see how such agreement can arise except fortuitously (from compensation among errors) because those calculations also neglected nuclear vibration.

Shape resonances in the scattering cross section are often correlated with unbound, unoccupied valence orbitals [50]. Taking this view, we would, for example, expect an A_1 resonance and a triply degenerate T_2 resonance in CF_4, both arising from C-F σ^* virtual valence orbitals, while in the H-containing fluoromethanes, we would expect not only C-F σ^* resonances in the appropriate IR's but also, at higher energies, C-H σ^* resonances. In conjunction with their electron-transmission measurements of resonance positions, Modelli *et al.* [51] carried out calculations based on this picture and predicted the energies of shape resonances in all of the fluoromethanes; however, both their measurements and their calculations were restricted to energies below ~ 11 eV, and all of the resonances their calculations predicted were of C-F σ^* type. Table XVIII compares the results of the present work to those of Modelli *et al.*, while in Fig. 10, we plot relevant symmetry components of our SEP ICS.

From Fig. 10, we see that the expected A_1 and T_2 resonances are observed in CF_4, occurring in the A_1 and B_2 IR's of C_{2v}. For CHF_3, we see an A_1 resonance at 9.3 eV and an E resonance at 10.8 eV, in fair agreement with Modelli *et al.*, who predicted 9.64 eV and 9.44 eV, respectively, for the A_1 and E resonance energies. We also see a pronounced A_1 resonance at 13 eV, which, on the basis of both energy and symmetry, may tentatively be assigned as the C-H σ^* resonance. In CH_2F_2, C-F σ^* resonances are expected in the A_1 and B_2 IR's, with predicted energies [51] of 10.17 and 9.44 eV, respectively; our SEP calculation shows a broad shoulder in the A_1 IR around 10.5 eV and a broad maximum in B_2 centered near 11.5 eV. No evidence of C-H σ^* resonances, which should occur in A_1 and B_1, is seen below 15 eV. For CH_3F, we see a weak maximum in A_1 near 9.5 eV, in fair agreement with the energy of 10.12 eV predicted for the C-F σ^* resonance by Modelli *et al.* As in CH_2F_2, there is no clear sign of the C-H resonances, indicating that they either lie above 15 eV or else are too broad to notice.

It is worthwhile observing that minimal-basis-set (STO-6G) RHF calculations show the energies of the C-F σ^* orbitals to be essentially independent of the degree of F substitution, occurring at 0.59 (T_2) and 0.62 (A_1) hartree in CF_4, at 0.57 (E) and 0.62 (A_1) hartree in CHF_3, at 0.58 (B_2) and 0.59 (A_1) hartree in CH_2F_2, and at 0.57 hartree in CH_3F. In contrast, the C-H σ^* orbital energies rise as the number of F atoms decreases, from 0.64 hartree in CHF_3, to 0.68 (B_1) and 0.69 (A_1) hartree in CH_2F_2, to 0.68 (E) and 0.70 (A_1) hartree in CH_3F, and to 0.71 (T_2) and 0.74 (A_1) hartree in CH_4. This trend may be understood as the C-H bonding orbitals being stabilized, and their conjugate σ^* orbital correspondingly destabilized, by the removal of electronegative substituents from the C center. This simple picture fits the pattern seen in our calculations quite well, i.e. all of the C-F resonances appearing to fall in the 9–12 eV range and only CHF_3 showing signs of a C-H resonance below 15 eV.

It was noted above and in an earlier work [17] that the DCS of the CH_xF_y molecules exhibit fluorination effects. Perhaps the clearest such effect occurs at energies around 30 eV: whereas the DCS of CH_4 at these energies is smooth in the 40–90° angular range, a weak feature appears near 60° in the CH_3F DCS, and this feature becomes a pronounced peak as one proceeds along the series through CH_2F_2 and CHF_3 to the fully F-substituted CF_4. This fluorination effect does not seem to be restricted to the fluoromethanes. For example, we see similar peaks in the DCS of 1,1,1,2-tetrafluoroethane ($C_2H_2F_4$) [53], C_2HF_5 [54], and C_2F_6 [53,55,56], but not in the DCS of C_2H_6 [57]; and likewise in the DCS of C_3F_8 [58,59], but not in that of C_3H_8 [53,60,61]. One is thus tempted to interpret this feature as due to the C-F atom pair, perhaps arising from a multiple-scattering effect. However, although the evidence is as yet limited, this fluorination effect appears to be either greatly weakened or inoperative in unsaturated fluorocarbons such as C_2F_4 [62] and 1,3-hexafluorobutadiene (C_4F_6) [53], despite the similarity in C-F bond lengths. A more detailed study of the electron

scattering process—looking, for example, at the body-frame or oriented-molecule differential cross sections—would perhaps help in clarifying the origin of this effect.

VII. SUMMARY

We have presented measured and calculated elastic electron cross sections for the fluoromethanes (CH_3F, CH_2F_2, CHF_3, and CF_4). Calculated results were obtained with the SMC method, employing a dipole-Born-closure procedure to improve the description of small-angle scattering by the polar molecules, and measured cross sections by a crossed-beam technique. Formal divergence of the Born-corrected results for the symmetric-top species (CH_3F and CHF_3) was avoided by taking the initial state to be $J=0,K=0$ in computing the rotationally summed cross section. For the hydrogen-containing species, the present calculated and experimental DCS agree well with each other. To obtain reasonable agreement with the experimental DCS of polar molecules at all angles, we found it necessary to include in the calculations both the longer-range interaction between the electron and the permanent dipole moment of the molecule and the shorter-range interaction between the electron and the induced dipole moment (the polarization interaction), except possibly in the case of CH_2F_2, where polarization appears to be relatively unimportant. A puzzling inconsistency exists between the present elastic ICS and measurements of the TCS below 5 eV for CH_3F and CHF_3. We obtained reasonably good calculated cross sections for CF_4, although a better description of polarization is needed. We also observed shape resonances for all fluoromethanes, with the possible exception of CH_3F. The present calculated resonance positions are in reasonable agreement with predictions of Modelli *et al.* [51], based on electron attachment energy calculations. With guidance from molecular orbital theory and from comparison with the calculations of Modelli *et al.*, all of the resonances observed may be assigned as C-F σ^*, with the exception of an apparent C-H σ^* resonance in CHF_3 near 13 eV.

ACKNOWLEDGMENTS

M.T.N.V. acknowledges support from Brazilian agency Fundação de Amparo à Pesquisa do Estado de São Paulo (FAPESP). C.W. and V.M. acknowledge support from the Department of Energy, Office of Energy Research. The authors acknowledge use of the facilities of the Center for Advanced Computing Research (CACR) at the California Institute of Technology, and the valuable assistance of the CACR staff, in particular, Heidi Lorenz-Wirzba. CACR is supported in part by the National Science Foundation through NPACI. M.T.N.V. would like to express his gratitude to Professor V. McKoy, Dr. C. Winstead, and Dr. K. Wang for their hospitality and friendship during his visit to the California Institute of Technology.

[1] L.G. Christophorou, J.K. Olthoff, and M.V.V.S. Rao, J. Phys. Chem. Ref. Data **25**, 1341 (1996).
[2] L.G. Christophorou, J.K. Olthoff, and M.V.V.S. Rao, J. Phys. Chem. Ref. Data **26**, 15 (1997).
[3] J. Moxom, J. Xu, G. Laricchia, L.D. Hullet, D.M. Schrader, Y. Kobayashi, B. Somieski, and T.A. Lewis, Nucl. Instrum. Methods Phys. Res. B **143**, 112 (1998).
[4] S. Motlagh and J.H. Moore, J. Chem. Phys. **109**, 432 (1998).
[5] K.N. Joshipura and M. Vinodkumar, Eur. Phys. J. D **5**, 229 (1999).
[6] A.M. Krzysztofowicz and C. Szmytkowski, J. Phys. B **28**, 1593 (1995).
[7] M. Kimura, O. Sueoka, A. Hamada, and Y. Itikawa, Adv. Chem. Phys. **111**, 537 (2000).
[8] T. Nishimura, J. Phys. B **31**, 3471 (1998).
[9] M. Goto, K. Nakamura, H. Toyoda, and H. Sugai, Jpn. J. Appl. Phys., Part 1 **33**, 3602 (1994).
[10] O. Sueoka, H. Takaki, A. Hamada, H. Sato, and M. Kimura, Chem. Phys. Lett. **288**, 124 (1998).
[11] J.E. Sanabia, G.D. Cooper, J.A. Tossell, and J.H. Moore, J. Chem. Phys. **108**, 389 (1998).
[12] R.B. Diniz, M.A.P. Lima, and F.J. da Paixão, J. Phys. B **32**, L539 (1999).
[13] L. Mi and R.A. Bonham, J. Chem. Phys. **108**, 1910 (1998).
[14] F.A. Gianturco, R.R. Lucchese, and N. Sanna, J. Chem. Phys. **104**, 6482 (1996).
[15] W.A. Isaacs, C.W. McCurdy, and T.N. Rescigno, Phys. Rev. A **58**, 309 (1998).
[16] M.T. do N. Varella, A.P.P. Natalense, M.H.F. Bettega, and M.A.P. Lima, Phys. Rev. A **60**, 3684 (1999).
[17] H. Tanaka, T. Masai, M. Kimura, T. Nishimura, and Y. Itikawa, Phys. Rev. A **56**, R3338 (1997).
[18] A.P.P. Natalense, M.H.F. Bettega, L.G. Ferreira, and M.A.P. Lima, Phys. Rev. A **59**, 879 (1999).
[19] K. Takatsuka and V. McKoy, Phys. Rev. A **24**, 2473 (1981); *ibid.* **30**, 1734 (1984).
[20] M.A.P. Lima and V. McKoy, Phys. Rev. A **30**, 501 (1988).
[21] C. Winstead and V. McKoy, Adv. At., Mol., Opt. Phys. **36**, 183 (1996).
[22] D.W. Norcross and N.T. Padial, Phys. Rev. A **25**, 226 (1982).
[23] T.N. Rescigno and B.I. Schneider, Phys. Rev. A **45**, 2894 (1992).
[24] S. Altshuler, Phys. Rev. **107**, 114 (1957).
[25] O.H. Crawford, A. Dalgarno, and P.B. Hays, Mol. Phys. **13**, 181 (1967).
[26] O.H. Crawford, J. Chem. Phys. **47**, 1100 (1967).
[27] Y. Itikawa and K. Takayanagi, J. Phys. Soc. Jpn. **26**, 1254 (1969).
[28] L. Boesten, H. Tanaka, A. Kobayashi, M.A. Dillon, and M. Kimura, J. Phys. B **25**, 1607 (1992).
[29] M.T. do N. Varella, M.H.F. Bettega, A.J.R. da Silva, and M.A.P. Lima, J. Chem. Phys. **110**, 2452 (1999).
[30] M.T. do N. Varella, M.H.F. Bettega, L.G. Ferreira, and M.A.P. Lima, J. Chem. Phys. **111**, 6396 (1999).
[31] D.M. Chase, Phys. Rev. **104**, 838 (1956).

[32] Yu. D. Oksyuk, Zh. Éksp. Teor. Fiz. **49**, 1261 (1965) [Sov. Phys. JETP **22**, 373 (1966)].
[33] K. Takayanagi, Prog. Theor. Phys. Suppl. **40**, 216 (1967).
[34] Y. Itikawa, J. Phys. Soc. Jpn. **30**, 835 (1971).
[35] T.N. Rescigno, B.H. Lengsfield, C.W. McCurdy, and S.D. Parker, Phys. Rev. A **45**, 7800 (1992).
[36] *CRC Handbook of Chemistry and Physics*, 78th ed. (CRC Boca Raton, 1997), pp. 9–45.
[37] M.W. Schmidt, K.K. Baldridge, J.A. Boatz, S.T. Elbert, M.S. Gordon, J.H. Jensen, S. Koseki, N. Matsunaga, K.A. Nguyen, S.J. Su, T.L. Windus, M. Dupuis, and J.A. Montgomery, J. Comput. Chem. **14**, 1347 (1998).
[38] T.N. Rescigno, B. H. Lengsfield, and C.W. McCurdy, in *Modern Electronic Structure Theory*, edited by D.F. Yarkony (World Scientific, Singapore, 1995), Pt. I, p. 501.
[39] S.L. Altman, Proc. Cambridge Philos. Soc. **53**, 343 (1957).
[40] H. Tanaka, L. Boesten, D. Matsunaga, and T. Kudo, J. Phys. B **21**, 1255 (1988).
[41] S. Srivastava, A. Chutjian, and S. Trajmar, J. Chem. Phys. **63**, 2659 (1975).
[42] *CRC Handbook of Chemistry and Physics*, edited by D.R. Lide, 81st ed. (CRC Press, Boca Raton, 2000), pp. 6–51.
[43] C. Winstead, Q. Sun, and V. McKoy, J. Chem. Phys. **98**, 1105 (1993).
[44] A.P.P. Natalense, M.H.F. Bettega, L.G. Ferreira, and M.A.P. Lima, Phys. Rev. A **52**, R1 (1995).
[45] L. Boesten, H. Tanaka, A. Kobayashi, M.A. Dillon, and M. Kimura, J. Phys. B **25**, 1607 (1992).
[46] A. Mann and F. Linder, J. Phys. B **25**, 533 (1992); *ibid.* **25**, 545 (1992).
[47] O. Sueoka, S. Mori, and A. Hamada, J. Phys. B **27**, 1453 (1994).
[48] C. Szmytkowski, A. Krzysztofowicz, P. Janicki, and L. Rosenthal, Chem. Phys. Lett. **199**, 191 (1992).
[49] R.K. Jones, J. Chem. Phys. **84**, 813 (1986).
[50] K.D. Jordan and P.D. Burrow, Acc. Chem. Res. **11**, 341 (1978).
[51] A. Modelli, F. Scagnolari, G. Distefano, D. Jones, and M. Guerra, J. Chem. Phys. **96**, 2061 (1992).
[52] A.P.P. Natalense, M.T. do N. Varella, M.H.F. Bettega, L.G. Ferreira, and M.A.P. Lima, J. Phys. B **32**, 5523 (1999).
[53] C. Winstead and V. McKoy (unpublished).
[54] M.H.F. Bettega, C. Winstead, and V. McKoy, J. Chem. Phys. **114**, 6672 (2001).
[55] T. Takagi, L. Boesten, H. Tanaka, and M.A. Dillon, J. Phys. B **27**, 5389 (1994).
[56] V. McKoy, C. Winstead, and C.-H. Lee, J. Vac. Sci. Technol. A **16**, 324 (1998).
[57] H. Tanaka, L. Boesten, D. Matsunaga, and T. Kudo, J. Phys. B **21**, 1255 (1988).
[58] H. Tanaka, Y. Tachibana, M. Kitajima, O. Sueoka, H. Takaki, A. Hamada, and M. Kimura, Phys. Rev. A **59**, 2006 (1999).
[59] C.-H. Lee, Ph. D. dissertation, California Institute of Technology, 1999.
[60] L. Boesten, M.A. Dillon, H. Tanaka, M. Kimura, and H. Sato, J. Phys. B **27**, 1845 (1994).
[61] C. Winstead, P.G. Hipes, M.A.P. Lima, and V. McKoy, J. Chem. Phys. **94**, 5455 (1991).
[62] C. Winstead and V. McKoy, J. Chem. Phys. (to be published).